

Spatio-temporal variability of CO₂ fluxes in the Atlantic sector of the Southern Ocean

Gabrielle Tavares de Carvalho¹, Luciano Ponzi Pezzi¹, Nathalie Lefèvre², Celina Cândida Ferreira Rodrigues¹, Marcelo Freitas Santini¹, Carlos Mejia².

¹Laboratory of Ocean and Atmosphere Studies (LOA), Earth Observation and Geoinformatics Division (OBT), National Institute for Space Research (INPE). Av. dos Astronautas, 1758, 12227-010, São José dos Campos, São Paulo, Brazil.

²Laboratoire d'Océanographie et du Climat: Expérimentations et Approches Numériques, Sorbonne Université/CNRS/IRD/MNHN, Institut Pierre-Simon Laplace - IPSL, Place Jussieu, 4, 75252, Paris, France

Corresponding author: Gabrielle Carvalho gabbytavares2011@hotmail.com (G. T. Carvalho).

† Av. dos Astronautas 1758, São José dos Campos 12227-010, São Paulo, Brazil.

Key Points:

- The CO₂ flux varies from -0.05 to 0.05 gC m⁻²month⁻¹ in the Atlantic sector of the Southern Ocean, depending on the seasons, from 2003 to 2022.
- The formation and melting of the sea ice cover has a strong influence on the variation in CO₂ absorption.
- The intensification of westerly winds on circumpolar oceanic fronts has intensified the absorption of CO₂.

Abstract

The Southern Ocean (SO) plays a fundamental role in the planet's climate system, due to its ability to absorb and redistribute heat and CO₂ (an important greenhouse gas). Besides, the SO interconnects three large oceanic basins the Pacific, the Atlantic, and the Indian Oceans, and it has an important role in the nutrient distribution into these oceans. However, the SO is poorly sampled with most measurements made in austral spring and summer. The variability of the air-sea CO₂ flux is estimated, as well as the role of atmospheric and oceanic variables in this variability. The CO₂ fluxes are calculated by the bulk parameterization method, in the Atlantic sector of the Southern Ocean, from 2003 to 2022, using *in situ* measurements, satellites and reanalysis data set. A neural network model is built to produce maps of the partial pressure of CO₂ in seawater (pCO_{2,sea}). The CO₂ flux varies from -0.05 to 0.05 gC m⁻² month⁻¹. The Atlantic sector of the SO is a sink of CO₂ in summer and spring and becomes a source in austral winter and autumn. The CO₂ absorption intensifies from 2003 to 2022 by 7.6 mmol m⁻²month⁻¹, due stronger westerly winds, related to the trend of the positive phase of the Antarctic Oscillation and the extreme events of El Niño and La Niña.

Plain Language Summary

The Southern Ocean (SO) plays a fundamental role in the planet's climate, due to its strong circulation of ocean waters, thus regulating heat and carbon reservoirs. The SO is an important CO₂ sink for the atmosphere. However, the amount of absorbed CO₂ varies over time, which is still poorly understood. The SO is not well sampled, due to difficulties in accessing the region and inhospitable climate. Most cruises are carried out in the austral spring and summer. Here we use *in situ* data, satellites, and modeled data to estimate the variability of the air-sea CO₂ flux, and the role of atmospheric and oceanic variables, in the Atlantic sector of the SO from 2003 to 2022. The CO₂ flux is calculated using the difference of partial pressure between the ocean and the atmosphere (bulk method). The CO₂ flux varies from -0.05 to 0.05 gC m⁻² month⁻¹, with the strongest absorption occurring mainly in summer and spring. The absorption of CO₂ from 2003 to 2022 has intensified, due to the increase in wind speed in the region, related to atmospheric and oceanic climate conditions.

1 Introduction

The Southern Ocean (SO) is considered an important CO₂ sink area, with an absorption of -1.0 Pg C/year (Landschützer et al., 2013). The main cause is the cold waters of the region, which results in greater CO₂ solubility (Silva et al., 2017, Rodrigues et al., 2023). In the SO, there is an intense transformation and formation of water masses, with a strong seasonality (Santini et al., 2018) which helps to control oceanic carbon reservoirs (Goldemberg et al., 2011).

The CO₂ flux (FCO₂) exchange between the ocean and the atmosphere varies in time and space (Landschützer et al., 2015; Sutton et al., 2021). The oceanic mesoscale may play a crucial role in

these flux exchanges. For example, Pezzi et al. (2021) showed that sea surface temperature (SST) anomalies caused by a warm core eddy (WCE) in the Southwestern Atlantic Ocean (SWA) near the SO, exerted a crucial influence on modifying the marine atmospheric boundary layer (MABL) by transferring heat and CO₂ from the ocean to the atmosphere. The WCE presence in midlatitudes, surrounded by predominantly cold waters, caused the ocean to act locally as a CO₂ source. Rodrigues et al. (2024) found that the intense horizontal gradient of SST combined with moderate wind and turbulence, in the Brazil Malvinas Confluence, modulates FCO₂, and leading to a CO₂ sink. Seasonal variations are explained by SST variations and biological activity (Landschützer et al., 2015; Sutton et al., 2021). Interannual and decadal variations may be related to changes in deep water formation and are associated with the Antarctic Oscillation (AO) and the El Niño-Southern Oscillation (ENSO) (Heinze et al., 2015; Brown et al., 2019; Avelina et al., 2020). Nevertheless, the magnitude of the influence of ENSO and AO on FCO₂ variability is still not understood (Sutton et al., 2021).

The ENSO, despite occurring in equatorial regions, influences the SST variability and the wind field in some regions of the SO, due to Rossby waves propagation. These waves are generated through vorticity from adiabatic heating, which, when moving south, induce teleconnections between ENSO and the SO climate (Parkinson and Cavalieri, 2012; Parkinson, 2019). ENSO has a La Niña phase (cold phase) and an El Niño phase (warm phase) (Lovenduski et al., 2008). AO is represented by an oscillation in surface pressure systems between medium and high latitudes in the Southern Hemisphere, having positive and negative phases (Thompson and Wallace, 2000). The Antarctic Oscillation is usually defined as the difference in the zonal mean sea level pressure at 40°S (mid-latitudes) and 65°S (Antarctica) (Fogt and Marshall, 2020).

The positive AO phase is defined by negative anomalies of geopotential height and temperature, in addition to the increase in the strength of the westerlies that lead to a greater upwelling of carbon from the ocean depths to the surface, which reduces the absorption of CO₂. The opposite occurs in the negative AO phase (Scholfield et al., 2018; Keppler and Landschützer, 2019; Nevison et al., 2020). During El Niño, there is an increase in the mixing of Circumpolar Deep Water (CDW) with Dense Shelf Water (DSW) advected from the Weddell Sea, leading to greater absorption of CO₂. The opposite occurs during La Niña (Keppler and landschützer, 2019; Brown et al., 2019; Nevison et al., 2020; Costa et al., 2020; Avelina et al., 2020).

The SO location, the high seasonality and ice cover, make it difficult to carry out oceanographic cruises, generating a lack of spatio-temporal information from the existing data set (Takahashi et al., 2009; Sabine et al., 2013; Bakker et al., 2016). There are few measurements in autumn and winter, most of them are made in austral summer and spring (Parkinson et al., 2012; Meijers et al., 2014; Monteiro et al. 2020). This makes it necessary to use tools that interpolate available measurements.

Here we use *in situ* data from the unprecedented collections of the Antarctic Modeling and Observation System (ATMOS) project, the Surface Ocean CO₂ Atlas (SOCAT) (<https://www.socat.info>), satellite and reanalysis datasets to estimate the air-sea CO₂ flux and its variability from 2003 to 2022. As pCO_{2,sea} is not available from satellite, we build an Artificial Neural Network (ANN) model to produce maps of pCO_{2,sea}. The ANN has become an increasingly efficient tool in the field of CO₂ studies and has been applied in estimations of pCO_{2,sea} and CO₂

fugacity (Landshutzer et al., 2013; Zeng et al., 2014; Hadjer et al., 2016). In addition, it performs better than linear regressions (Hadjer et al., 2016).

Thus, this study contributes to increase our knowledge of the spatio-temporal variability of the FCO₂ in the Atlantic sector of the Southern Ocean, as well as the role of atmospheric and oceanic variables in explaining this variability. From this, it becomes possible to understand the causes of the intensification of the CO₂ absorption, as well as the consequences for the studied region.

Section 2 describes the methodology and the data. Section 3 brings the main results found in this study. Section 4 discusses the analysis carried out and, finally, Section 5 presents the conclusions of this work.

2 Materials and Methods

The study area is presented in section 2.1, followed by in situ data (section 2.2) related to the ATMOS Project, satellite and reanalysis data set (section 2.3). Direct measurements of CO₂ fluxes obtained from the ATMOS oceanographic cruise are described in Section 2.4. The training of the neural network based on ATMOS and SOCAT data set is described in Section 2.5. The CO₂ flux data estimated from the bulk parameterization is described in section 2.6. Finally, the FCO₂ variability analysis technique is described in section 2.7.

2.1 Study area

The SO has the largest and fastest ocean current on the globe, the Antarctic Circumpolar Current (ACC), driven by the strong easterly winds characteristic of southern polar latitudes (Orsi et al. 1995; Klinck and Nowlin, 2001; Barke et al., 2007). The oceanic circulation of the SO occurs as follows: the upper cell of the meridional circulation is driven by wind, which causes upwelling of the CDW along inclined isopycnals, due to divergent Ekman transport, which upwells in the ACC (Marshall et al., 2012). At the surface, CDWs become Subantarctic Modal Waters (SMW) and Antarctic Intermediate Waters (AIWs), which makes the upper part of the Southern Overturning Circulation (Sallée et al., 2010). Surface buoyancy flows, ocean-atmosphere interactions, ice shelves, and sea ice produce cold, salty Dense Shelf Water (DSW). DSW becomes the dense Antarctic Bottom Water (ABW), formed in seas such as the Ross and Weddell seas, and along the east coast of Antarctica (Ohshima et al., 2013).

When the ACC reaches the Drake Passage, the narrowing between Antarctica Peninsula and southern end of South America causes an increase in the ACC speed, and results in the strengthening of the main circumpolar oceanic fronts present in the region (Figure 1, Sprintall, 2003). These fronts, from south to north, are: 1) the Southern Boundary (BF), which is the northern limit of the cold water mass; 2) the Southern Antarctic Circumpolar Current Front (SACCF), which extends approximately along the Antarctic slope and deviates slightly northwards at 56° W; 3) the Polar Front (PF), formed by the convergence of Antarctic and subantarctic waters, and 4) the Subantarctic Front (SAF) which defines the northern boundary of the ACC. To the north of the SAF is the Subtropical Front (STF), which marks the northernmost extent of subantarctic waters (Orsi et al. 1995).

Around Antarctica there is a cover of sea ice, which varies seasonally. During the warm season it reduces, due to melting (minimum in February), and during the cold season it expands, due to

freezing (maximum in September) (Parkinson and Cavalieri, 2012; Parkinson, 2019). In addition to the aforementioned factors that can affect the FCO₂, there is also the passage of atmospheric cold fronts. Indeed, the fronts cause changes in the surface wind field, pressure, temperature, and other atmospheric variables during their trajectory, in addition to their interactions with the sea surface (Wallace and Hobbs, 2006).

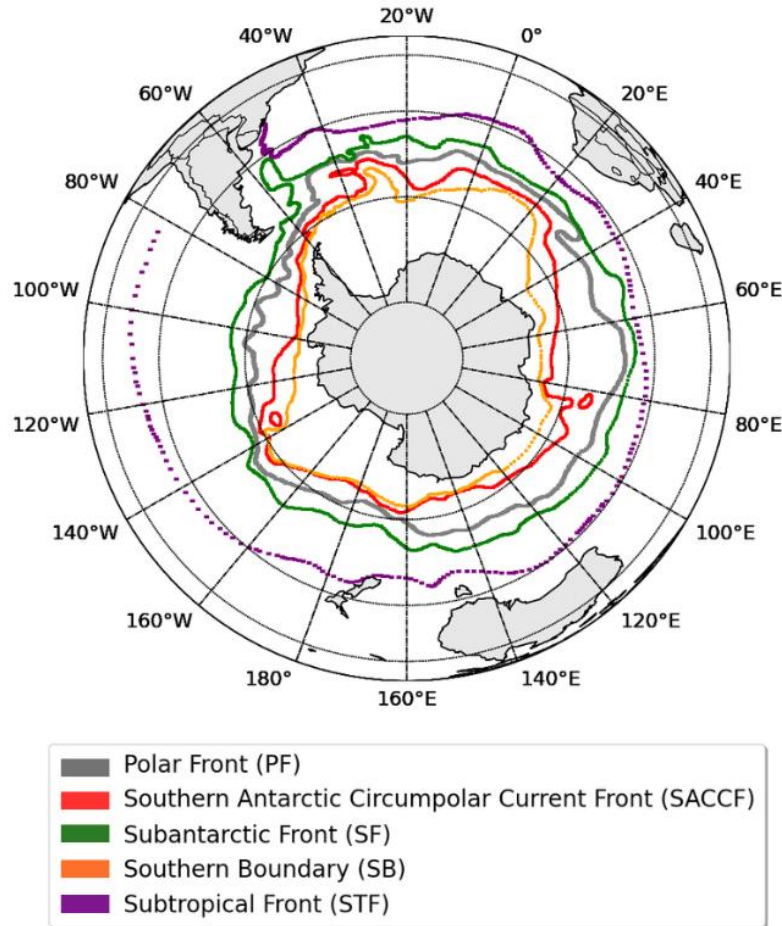


Figure 1 - Study area location in the Atlantic sector of the Southern Ocean. The isolines illustrate the circumpolar oceanic fronts from south to north, and they are the Southern Boundary (SB), the Southern Antarctic Circumpolar Current Front (SACCF), the Polar Front (PF), and the Subantarctic Front (SAF). To the north of the SAF is the Subtropical Front (STF) (Orsi et al. 1995).

2.2 *In situ* data

In situ data were obtained from the ATMOS project (Table 1). The oceanographic cruise occurred during OPERANTAR XL, aboard Brazilian Navy Polar Vessel (Po/V) Almirante Maximiano (H-41), between November 2021 and February 2022 (Pezzi et al. 2021; Voermans et al, 2021). The data was collected by sensors installed in the meteorological tower at the bow of the ship (available

in Carvalho, G. T., & Pezzi, L. P., 2024), and data measured by LI-COR (LI-850) installed in the laboratory aft of the ship (available in Carvalho, G. T., & Pezzi, L. P., 2024) (Table 1).

The Sea Surface Salinity (SSS) data were interpolated from reprocessing systems that combine data from NASA's Soil Moisture Active Passive (SMAP) and European Space Agency's (ESA) Soil Moisture Ocean Salinity (SMOS) satellites and in situ measurements (<https://doi.org/10.48670/moi-00051>). The Sea Surface Temperature (SST) data are from the reprocessing of Along Track Scanning Radiometer (ATSR), Sea and Land Surface Temperature Radiometer (SLSTR) and Advanced Very High Resolution Radiometer (AVHRR) satellite data by the ESA SST Climate Change Initiative (CCI) and Climate Change Service (C3S) projects, they were produced from the Operational Sea Surface Temperature and Sea Ice Analysis system (OSTIA) (<https://doi.org/10.48670/moi-00169>).

SSS, SST, sea level pressure (SLP), H₂O and partial pressure of CO₂ gas in sea (pCO_{2sea}) were obtained from SOCAT. Interpolated Air temperature (T_{air}) and wind speed were obtained from the MERRA-2 satellite (https://disc.gsfc.nasa.gov/datasets/M2I1NXLFO_5.12.4). Interpolated concentrations of CO₂ (xCO_{2air}) were downloaded from Global View (<https://gml.noaa.gov/>). pCO_{2air} can be considered as the pressure that the gas is in equilibrium in the air, which it would exert on a surface of water containing dissolved CO₂. The pCO_{2air} was obtained from xCO_{2air}, Patm and pH₂O (Landshutzer et al., 2013).

Sensor	Model	Manufacturer	Variables sampled
Integrated CO ₂ /H ₂ O Open-path gas analyzer and 3D sonic anemometer	IRGASON	Campbell Scientific	CO ₂ density, H ₂ O density 3D wind components air temperature, air pressure
Multi axis inertial sensing system	Motion Pack II	Systron Donner Inertial	3D accelerations and 3D angular velocities
GPS	GPS16X-HVS	Garmin	Position

Infrared gas analyzer	LI-850	Li-cor Biogeosciences	CO ₂ concentrations in water
-----------------------	--------	--------------------------	--

Table 1. Meteorological and oceanic sensors installed on the micrometeorological tower and ship hull during the ATMOS cruise.

2.3 Satellite and reanalysis data set

A collection of satellites and reanalysis data set were used for the study of the Atlantic sector of the SO and for the FCO₂ estimation. The FCO₂ estimation was made using data set from satellite multi-sources to complete the time series for the period from 2003 to February 2022.

The satellite data used in this study were: The CO₂ estimates used are from the Atmospheric Infrared Sounder (AIRS) sensor, on board the Aqua satellite, with a spatial resolution of $2.5^{\circ} \times 2^{\circ}$, from 2003 to 2014 (https://disc.gsfc.nasa.gov/datasets/AIRX3C2M_005). The 2015 to 2022 CO₂ estimates are from the Orbiting Carbon Observatory - 2 (OCO-2) satellite, which provides estimations with a spatial resolution of $1.29 \text{ km} \times 2.25 \text{ km}$ (<https://disc.gsfc.nasa.gov/datasets?keywords=oco2>). The SLP, Tair and wind speed were obtained from the Modern-Era Retrospective analysis for Research and Applications, Version 2 (MERRA-2) satellite. With spatial resolution of $0.5^{\circ} \times 0.625^{\circ}$, from 2003 to 2022.

Monthly reanalysis SST and SSS were obtained from Multi Observation Global Ocean ARMOR3D (<https://doi.org/10.48670/moi-00052>). These analyses combine satellite data from Advanced Very High Resolution Radiometer (AVHRR) and Advanced Microwave Scanning Radiometer-2 (AMSR-2), and in situ observations distributed by NOAA's National Climatic Data Center, with a spatial resolution of $0.25^{\circ} \times 0.25^{\circ}$, from 2003 to 2022. The Chlorophyll products used in this work are from Global Ocean Color (<https://doi.org/10.48670/moi-00052>), with spatial resolution of 4 km. This product uses data from several satellites, such as Sea-viewing Wide Field-of-view Sensor (SeaWiFS), Moderate-Resolution Imaging Spectroradiometer (MODIS), Medium Resolution Imaging Spectrometer (MERIS), Visible Infrared Imaging Radiometer Suite sensor (VIIRS) aboard the Suomi-National Polar-orbiting Partnership (SNPP), Joint Polar Satellite System-1 (JPSS1), Ocean Land Color Imager (OLCI) aboard the Sentinel-3A (S3A) and Sentinel-3B (S3B).

2.4 Eddy Covariance Method

Eddy Covariance (EC) is the method used to obtain direct measurements of turbulent fluxes from the covariance between the fluctuations in the mean CO₂ density and the vertical component of the wind, thus providing the flux of CO₂ between the ocean surface and the atmosphere as indicated in the Equation 1 (Miller et al., 2010; Pezzi et al 2016; Santini et al., 2020). These measurements are made at high temporal frequencies and are performed in the surface layer of the Marine Atmospheric Boundary Layer (MABL) (Mcgillis et al., 2001, Pezzi et al., 2021). The MABL is the layer nearest to the ocean surface, which is where momentum, heat and gas exchange take place (Foken et al., 2008). The EC has already been used in previous studies in the Southwestern Atlantic such as Pezzi et al. (2016), Santini et al., (2020) and Pezzi et al, (2021) to study the MABL

stability. The role of roughness and stability on momentum fluxes at Brazil-Malvinas Confluence was studied in Hackerott et al. (2018). Recently Pezzi et al. (2021) studied the turbulence and instability of the MABL caused by an oceanic WCE and consequent modification in the behavior of CO₂, heat and momentum fluxes in the BMC. Additional information about EC can be found in these cited articles, as the methodology employed here is the same.

The FCO₂ is given in $\mu\text{mol m}^{-2}\text{s}^{-1}$, by the fluctuations of the vertical wind component (w' in m/s) and the CO₂ mixing ratio (c' in mg/m³), in relation to their averages, and the average dry air density (ρ_a in $\mu\text{mol.m}^{-3}$):

$$\text{FCO}_2 = \rho_a \overline{w'c'} \quad (1)$$

The calculation of the FCO₂ was performed using the free open-source software EddyPro®v7.0.9, offered by LI-COR Biosciences Inc. (EddyPro v7.0.9). Fluxes are calculated using 30-minute averages of high-frequency (20 Hz) data. Before the FCO₂ estimation, the wind data were corrected due to the ship's movement (Miller et al. 2008; Rodrigues et al., 2023).

2.5 Artificial neural network to estimate pCO_{2sea}

The ocean CO₂ partial pressure (pCO_{2sea}) data are very sparse in the study area. Therefore, an Artificial Neural Network (ANN) was used to fill spatial and temporal gaps in pCO_{2sea} (Nakaoka et al., 2013; Landshutzer et. al., 2013). In this study, 279.480 observations from SOCAT and ATMOS over the 2003-2022 period, are used to reconstruct the pCO_{2sea} for the study region. The dataset is split into two distinct groups (Géron et al., 2017):

1) 85% of the data are randomly selected for utilization during the training phase. This will be identified as the Train set.

2) The remaining 15% are allocated for the neural network diagnosis phase. Called Test set.

The standard procedure of data normalization (scaling) is implemented on every input and output variable, aiming to achieve a mean of zero and a standard deviation of 1 for each of them. The network consists of an input layer composed of 3 neurons, 3 hidden layers with 10, 8 and 5 nodes respectively and an output layer, that is, the estimate of pCO_{2sea}, as shown in Figure 2. For the precision analysis of the pCO_{2sea} estimate, the mean squared error and Pearson's coefficient were defined (Géron et al., 2017). Previous studies that applied this methodology over the Atlantic Ocean used SST, SSS and chlorophyll in data input (Landshutzer et. al., 2013). However, in this study, during the initial tests to produce the model, the set of variables SST, SSS and pCO_{2air} (Figure 2a) proved to be more efficient in estimating pCO_{2sea} than the input data used by Landshutzer et. al., (2013). The Pearson correlation (r) showed that the variables SSS, SST and chlorophyll (Figure 2a) as input data for the ANN model, have $r = 0.59$ with the observed pCO_{2sea} data. While with SSS, SST and pCO_{2air} data (Figure 2b) the correlation is greater ($r = 0.69$). Furthermore, the root mean-square (RMS) error calculated based on the two sets of input data for the ANN was lower with the SSS, SST and pCO_{2air} data (RMS = 33.47) (Figure 2c), from than in relation to the set of SSS, SST and chlorophyll variables (RMS = 40.41) (Figure 2b). The model

was produced in the Python 3 programming language, available at Carvalho, G. T & Mejia, C., 2024. Two platforms were also installed: TensorFlow and Keras (Chollet et al., 2018).

The ANN estimates $p\text{CO}_{2\text{sea}}$. With $p\text{CO}_{2\text{sea}}$, it is then possible to calculate FCO_2 on a large spatial and temporal scale.

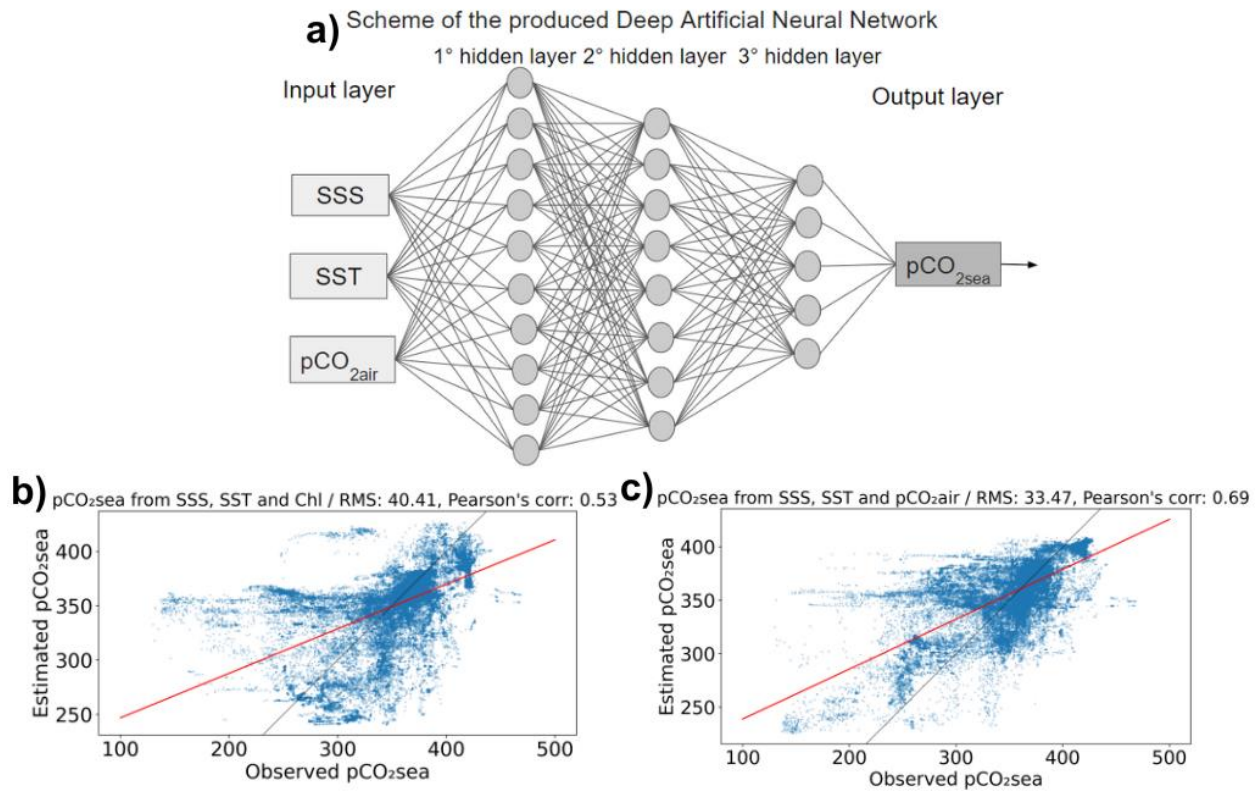


Figure 2 - a) Scheme of the produced Deep Artificial Neural Network. The input data are salinity (SSS) (psu) and sea surface temperature (SST) ($^{\circ}\text{C}$) and CO_2 partial pressure of air ($p\text{CO}_{2\text{air}}$) (μatm). The ANN includes 3 hidden layers with 10, 8 and 5 nodes. The output layer gives the seawater partial pressure of CO_2 ($p\text{CO}_{2\text{sea}}$) (μatm). b) Pearson correlation between $p\text{CO}_{2\text{sea}}$ estimates using SSS, SST and Chl as ANN input data. c) Pearson correlation between $p\text{CO}_{2\text{sea}}$ estimates using SSS, SST and $p\text{CO}_{2\text{air}}$ as ANN input data. Scatterplots and regression lines were calculated from Test data (with 15% of the data set).

2.6 Bulk parameterization

FCO_2 was determined by the bulk parameterization ($\text{FCO}_{2\text{BK}}$) shown in Equation 2, where $\text{FCO}_{2\text{BK}}$ is defined by the product of the ocean-atmosphere CO_2 partial pressure gradient $\Delta p\text{CO}_2$ ($\Delta p\text{CO}_2 =$

$p\text{CO}_{2\text{sea}} - p\text{CO}_{2\text{air}}$), the solubility (s) and the wind-dependent air-sea gas transfer velocity (K) (Farias et al., 2013; Ito et al., 2016):

$$\text{FCO}_{2\text{BK}} = s \cdot k \cdot \Delta p\text{CO}_2(\text{sea-air}) \quad (2)$$

The solubility (s) CO_2 in seawater was defined with the relationship used by Weiss, 1974. K was calculated according to Sweeney et al. (2007). The direction and part of the magnitude of FCO_2 are defined by $\Delta p\text{CO}_2$, whose variability is dominated by $p\text{CO}_{2\text{sea}}$ in our observations.

The bulk parameterization was applied using satellite and reanalysis data, from 2003 to 2022. Due to each of the satellite and reanalysis data having different spatial resolutions, as can be seen in Table 2, it was necessary to re-grid them. The interpolation was based on the spatial resolution of CO_2 observations from the AIRS and OCO-2 satellites. From 2003 to 2014 the data had a final spatial resolution of $2^\circ \times 2.5^\circ$, and from 2015 to 2022 the final spatial resolution was $0.5^\circ \times 0.625^\circ$. The interpolation was performed using the Cubic Convolution Interpolation tool applied using the Python 3 tool. In this method, the 16 closest pixels (4×4 window) are considered and the interpolation is performed by adjusting cubic polynomials to each column, to then interpolate a new cubic polynomial to these results. It is the most suitable method for studies that need to work with data at different resolutions (Cunha et al., 2012; Dourado et al., 2014).

2.7 CO_2 flux variability analysis

The analysis of FCO_2 in the Drake Passage covered the months of February of the years 2016 and 2019 based on bulk SOCAT data, and from 12/01/2021 to 02/15/2022 based on the ATMOS project collections (Pezzi et al., 2021; Voermans et al., 2021; Rodrigues et al., 2023), obtained by the Eddy Covariance (EC) method.

Afterwards, the bulk was applied again, but now with satellite data, reanalysis, and ANN, in the Atlantic sector of the Southern Ocean. Next, an analysis of the monthly FCO_2 series was carried out and the role of atmospheric and oceanic variables in FCO_2 variability was described. The influence of ENSO and AO on FCO_2 was also investigated. ENSO and AO information is available from the Climate Prediction Center (CPC), National Oceanic and Atmospheric Administration (NOAA) National Center for Environmental Prediction (NCEP) during the period 2003 to February 2022.

3 Results

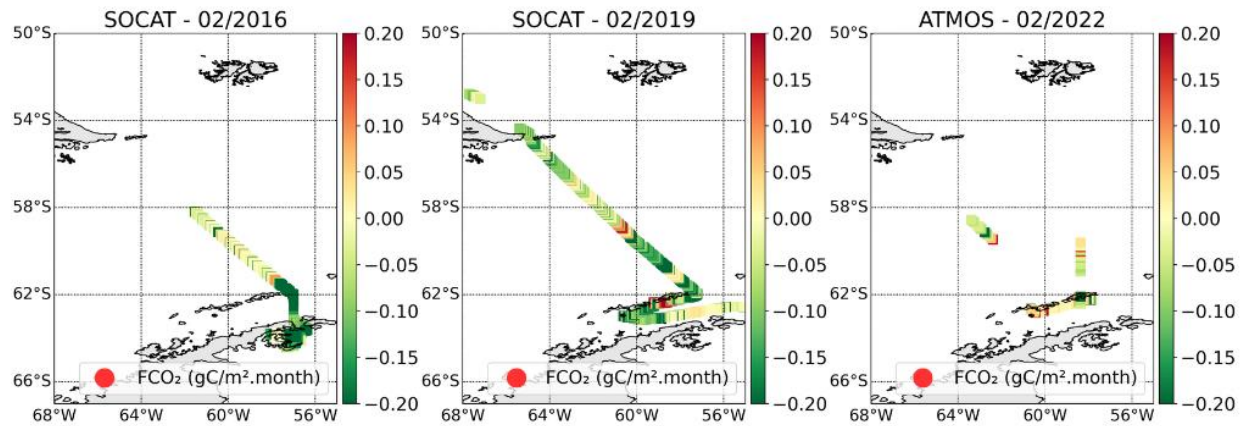
In this section we present the results of this study, based on in situ data collection, estimated flows and reanalysis data, in addition to flow estimates resulting from the artificial neural network model.

3.1 CO_2 flux variability in February

The monthly FCO_2 in the Drake Passage is presented for February of 2016, 2019 and 2022 (Figure 3). Using bulk parameterization with SOCAT data, it was $-0.01 \text{ gC m}^{-2}\text{month}^{-1}$ in 2016 and $-0.005 \text{ gC m}^{-2}\text{month}^{-1}$ in 2019. Using eddy covariance with ATMOS data in 2022, the flux was $-0.04 \text{ gC m}^{-2}\text{month}^{-1}$. Similar results were observed by Takahashi et al. (2009), with a flux of $-0.02 \text{ gC m}^{-2}\text{month}^{-1}$. These values were due to the Southern Ocean acting as a CO_2 sink during the austral summer (Dejong et al., 2017; Brown et al., 2019; Monteiro et al., 2020). This absorption in the

314 summer occurs because it is a period of increased availability of light and nutrients. Nutrients are
315 from upwelled Circumpolar Deep Waters, which leads to an increase phytoplankton blooms,
316 decreasing $p\text{CO}_{2\text{sea}}$, and increasing CO_2 uptake by the ocean (Ducklow et al., 2013; Heinze et al.,
317 2015; Viana et al., 2021). Despite the predominance of CO_2 absorption in the Drake Passage, there

318 is a release of CO₂ near 60°S observed with SOCAT and ATMOS data in 2019 and 2022 (Figure
319 3).



320

321 **Figure 3** - CO₂ fluxes in gC m⁻²month⁻¹ distribution at Drake Passage with SOCAT data for
322 February 2016 and 2019, and ATMOS data for February 2022.

323 3.3 FCO₂ calculated with artificial neural network.

324 The 2003–2022 average FCO₂, calculated from the maps of pCO_{2,sea}, was -0.027 gC m⁻²month⁻¹,
325 and from *in situ* data was -0.029 gC m⁻²month⁻¹, but the average bias is small (-0.002 gC m⁻²month⁻¹).
326 FCO₂ from *in situ* data (SOCAT and ATMOS data) was determined by the bulk method from
327 2003–2022. The comparison between the two fluxes can be seen in the Taylor diagram, which
328 provides a simple graphical representation of what the next one will bring from the other (Figure
329 4). In relation to the standard deviation of the observed data, it was 2.4 and that of the model was
330 1.7 (Figure 4). The root mean square error (RMS) error between the two was 1.5. The FCO₂, based
331 on the reconstruction of pCO_{2,sea}, may have overestimated the flow variability by 5.3%. However,
332 this underestimation is low, given what was observed by Gloege et al., (2021) for the Southern
333 Ocean, of 31%. The percentage overestimation is, by definition, inversely proportional to the
334 standard deviation of the model (GLOEGE et al., 2021). According to the dispersion of -0.013 gC
335 m⁻²month⁻¹, obtained by the absolute error, it indicates that the amplitude of the monthly variability
336 of the CO₂ flow produced may be close to the original. The correlation with the flow calculated
337 with *in situ* data was high ($r = 0.76$), being higher than that observed in Gloege et al., (2021) with
338 $r = 0.54$.

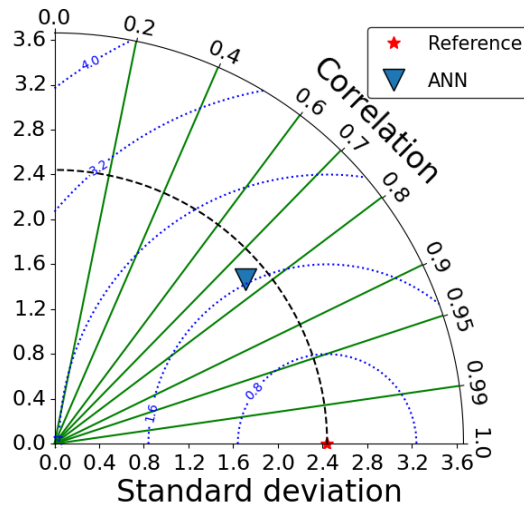


Figure 4 - Taylor diagram for comparison between the FCO_2 calculated with *in situ* data (Reference) and from the ANN $\text{pCO}_{2\text{sea}}$ reconstruction (ANN). The blue lines are the root-mean-square (RMS) error.

To detect possible increase or decrease of CO_2 absorption, we calculate the monthly CO_2 flux anomalies over 2003-2022 using the maps produced by the ANN (Figure 5).

The area from 40°S to 45°S exhibits large seasonal changes with positive flux in the months of December, January, February (austral summer) and in the months of September, October, and November (austral spring), and negative values in the months of June, July and August (austral winter) and in March, April and May (austral autumn). The region from 45°S to 55°S also exhibits seasonal changes, ranging from being a strong sink of CO_2 in summer and spring, and having reduced absorption in winter and autumn, indicating that it is a year-round sink. This zone is the Antarctic Divergence area, located within the high wind speed zone (40 - 60°S). The strong winds cause a large vertical mixing of seawater, which increases the exchange of CO_2 at the air-sea interface, explaining the strong CO_2 sink (Arrigo et al., 2007; Le Queré et al., 2007). In this region, the North Atlantic Deep Water resurfaces from 2000 m depth to 200 m, with higher temperatures (Tomczak; Godfrey, 1994). South of 55°S is an area of year-round CO_2 absorption. However, absorption is reduced in winter and autumn. During the southern spring-summer, phytoplankton blooms occur near the ice and increase the CO_2 absorption. This indicates the effect of ice cover on the FCO_2 in this region, as observed in Takahashi et al. (2009), Shetye et al. (2017) and Monteiro et al. (2020).

In summer, absorption is more intense than in other seasons (Figure 5), absorbing 72% more than in autumn and winter, and 51% more than in the southern spring. The absorption peak occurs mainly in February, and the lowest absorption values are mainly in August, in the study region. This is due to the expansion of sea ice cover that occurs in autumn and winter, with maximum expansion in August and September (Parkinson and Cavalieri, 2012; Parkinson, 2019). The ice cover can extend from the Antarctic continent to 55°S in the Atlantic sector in some years, however, on average it can extend up to 62°S in winter (Takahashi et al., 2009). As winter progresses, ice formation increases, releasing salts, which can contribute to the release of CO_2 into the water. The layer of mixed water under the ice is rich in CO_2 , mainly due to the vertical mixing

of deep waters (Nomura et al., 2006; Takahashi et al., 2009). However, in the summer and spring the ice cover melts, and reaches its minimum size in February, which is why this is the month in which the greatest absorption of CO₂ occurs (Wadhams, 2000). Furthermore, in the southern summer and spring there is an increase in light availability and stable stratification of surface water, which allows an increase in primary biological productivity, which leads to an increase in CO₂ absorption during these seasons (Ducklow et al., 2013; Heinze et al., 2015; Viana et al., 2021).

The FCO₂ varies from -0.05 to 0.05 gC m⁻²month⁻¹ in the Atlantic sector of the SO, absorbed in the summer and spring periods, and in the southern winter and autumn, absorption decreases. CO₂ absorption has intensified in the study area, with an increase of 0.076 gC m⁻²month⁻¹ from 2003 to 2022. This behavior is shaped by wind speed and SST, but mainly by the intensification of winds that increased during the studied period, which may be driven by climate variability (Marshall et al., 2003; Stammerjohn et al., 2008; Brown et al., 2008, 2019). Furthermore, an increasing trend in pCO_{2air} was also observed, which has been increasingly higher than in water. The increase in pCO_{2air} is due to anthropogenic CO₂ emissions. The rate of increase of pCO_{2sea} is slower in highly mixed regions as deeper waters with a lower CO₂ content are brought to the surface. In high stratified regions, the same rate of increase is observed in the ocean and in the atmosphere. Previous studies that modeled future scenarios already expected this response from the Southern Ocean to increased CO₂ emissions (Sabine; Cols., 2004; Friedlingstein et al., 2006; Roy et al., 2011; Arora et al., 2013; Steinacher et al., 2013; Zickfeld et al., 2013). These models predicted that in scenarios with high greenhouse gas emissions, there would be a reduction in the efficiency of absorption by the ocean. This occurs because the increase in atmospheric CO₂ concentration is linked to the increase in anthropogenic emissions. Thus, although absorption by the ocean has intensified, the ocean is not able to absorb all the excess CO₂ present in the atmosphere resulting from anthropogenic emissions.

In the Drake Passage, the absorption in the summer and spring periods is of -0.01 gC/m².month and -0.013 gC m⁻²month⁻¹, respectively. In the autumn and winter periods, there is a reduction in absorption of -0.012 gC m⁻²month⁻¹. Similar results were observed by Takahashi et al. (2009). In summer and spring, they observed strong CO₂ absorption, and in autumn and winter there is a reduction in absorption, being -0.09 gC m⁻²month⁻¹, -0.02 gC m⁻²month⁻¹, 0.01 gC m⁻²month⁻¹ and 0.013 gC m⁻²month⁻¹, respectively.

SST anomaly maps produced by reanalysis data (Figure 6) illustrate that some regions of the study area are becoming increasingly warmer over time, which affects FCO₂. The waters coming from the Pacific Ocean through the Drake Passage to the Atlantic sector of the Southern Ocean are releasing more CO₂ than the expected average (Figure 5). These waters are the waters of the PF. The PF is located approximately at latitude 50°S in the Atlantic oceans and at latitude 60°S in the Pacific, it is a region where CO₂ is released, due to its average surface temperature being higher than that south of this region. This behavior was also observed with SOCAT and ATMOS data (Figure 3). The surface water south of this region moves north and sinks when it reaches the PF, thus causing convergence at the surface (Pickard and Emery, 1990). However, with the increase in SST, the PF shows stronger CO₂ outgassing. To the north of the PF there is an increase in CO₂ release, this region has higher temperatures, due to the dominant effect of seasonal SST changes (Tomczak; Godfrey, 1994). However, to the south of the PF there is an increase in CO₂ absorption. In this region the surface waters of the Antarctic Zone have very low temperatures, reaching values close to the freezing point (-1,9°C), as a result of the summer melting of the sea ice and surface

413 cooling in winter (Tomczak; Godfrey, 1994). Below the surface in the Antarctic Zone, extending
414 up to 4000 m deep, is the Antarctic Circumpolar Water (AACW), with temperatures of 1.5 to 2.5°C
415 (Tomczak; Godfrey, 1994). Close to the coast of the Antarctic continent, some regions also
416 intensified the release of CO₂, despite being a region with a higher potential temperature than at
417 the shelf break, the SST was also warmer. This region is where the Deep Circumpolar Water rises
418 over the slope to enter the platform, it has warmer and saline waters (Baines, 2006). However, the
419 waters that are a source of CO₂, are expanding southward, and the waters that are sinks of CO₂
420 become stronger sinks. This is due to the increase in strength and southward displacement of the
421 westerly winds, associated with the positive trend of the AO, which forced the migration of the FS
422 towards the Antarctic continent, thus migrating warm and saline waters, which cause the release

of CO₂. This trend towards the positive phase of OA is due to the increase in greenhouse gases (Thompson; Solomon, 2002; Marshall et al., 2003; Cai et al., 2005; Cai; Cowan, 2007).

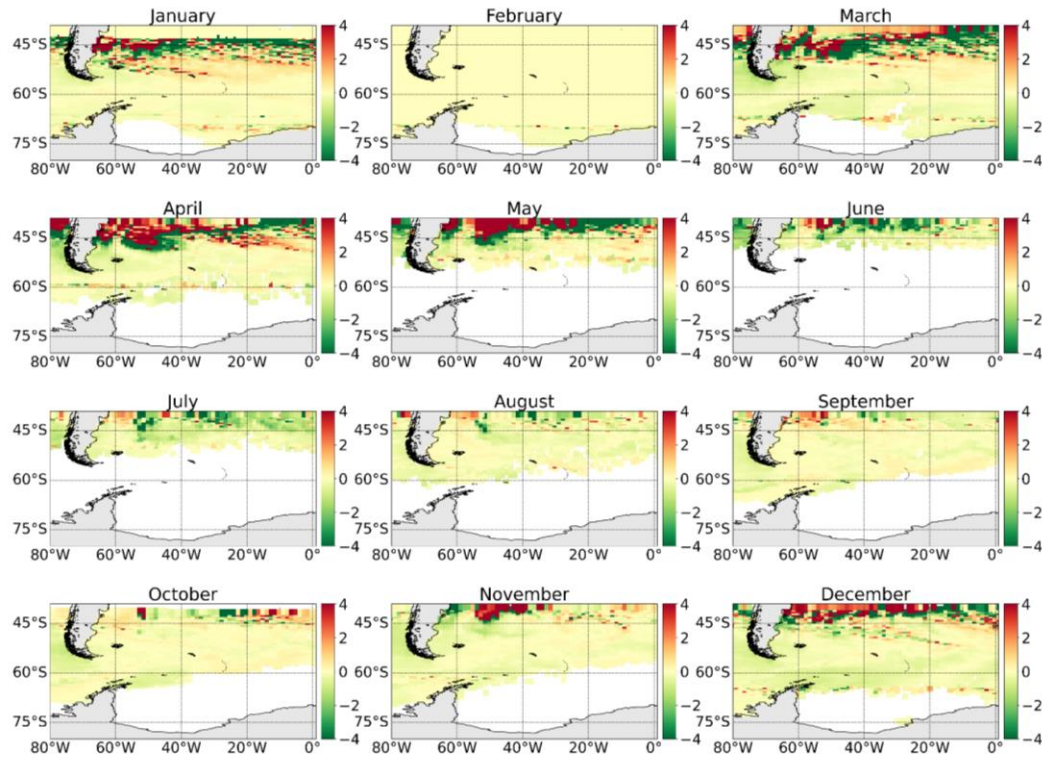


Figure 5 –Monthly anomalies of the CO₂ flux (in gC m⁻²month⁻¹) calculated from 2003 to 2022.

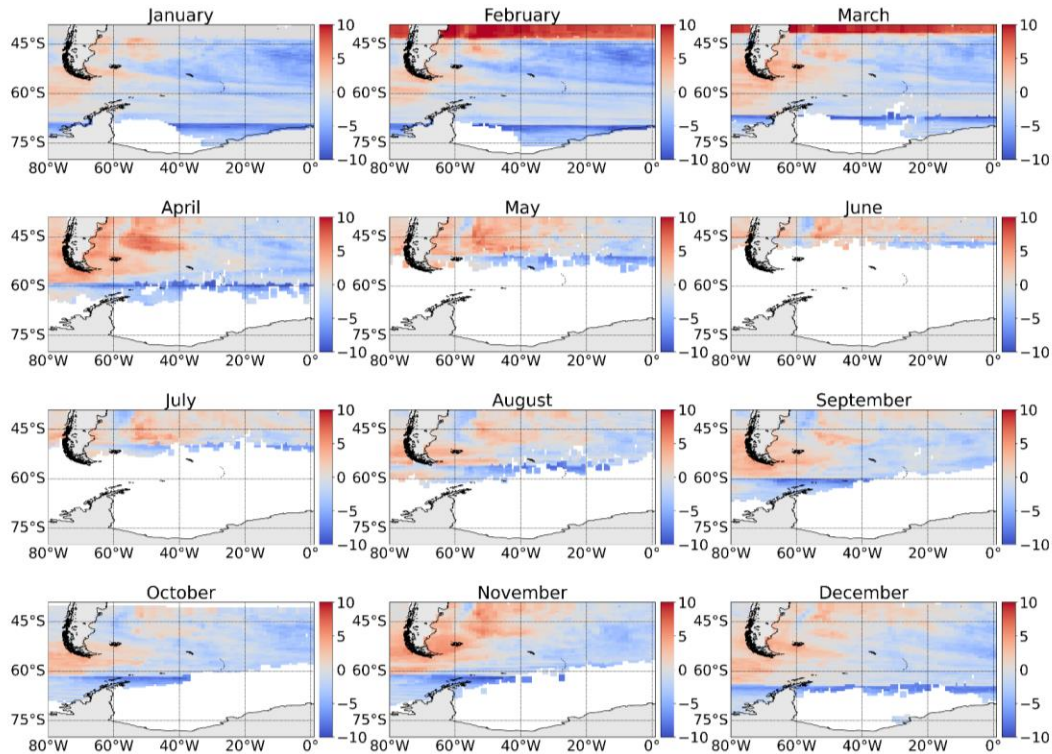


Figure 6 – Monthly sea surface temperature (°C) anomalies produced after reanalysis, from 2003 to 2022.

3.4 Variability of CO₂ flux

In the region between -63° to -54°W and -59° to -62°S, in the Drake Passage, an analysis of the temporal variability of FCO₂ and atmospheric and oceanic variables was carried out, including the climate indices ENSO and OA, based on the historical series from 2003 to 2022.

There is a tendency towards negative CO₂ values throughout the period studied (Figure 7a), with peaks and decreasing values, which follow the seasonality of the SST (Figure 7b). The SLP varies inversely to the temperature, that is, when the temperature increases the SLP decreases and vice versa (Figure 7e, 7b). Furthermore, the SLP appears to be inversely proportional to the FCO₂, so it is possible to observe that where there is a drop in the SLP, there is an increase in the values of FCO₂, which become more positive (Figure 7e). This relationship between SLP and FCO₂ indicates a decrease in the concentration of atmospheric CO₂ near the surface and, consequently, there is a tendency to transfer CO₂ from the ocean to the atmosphere. Wind speed is strongest in the months of March to November, ranging from 11-13 (m/s), and reduces in the months of December to February (southern summer), ranging from 9-10 (m/s) (Figure 7g). CHL varies seasonally, CHL blooms occur during the austral spring-summer, and reduce in the austral autumn-winter (Figure 7c). The months of August and September have the lowest concentrations of CHL.

It was observed from $\Delta p\text{CO}_2$ (Figure 7d), which defines the direction and part of the magnitude of FCO₂, that $p\text{CO}_{2\text{air}}$ is what dominates the variability of FCO₂ in this study. $\Delta p\text{CO}_2$ has a decreasing

trend, indicating that the direction of FCO_2 is towards the atmosphere towards the ocean. An increasing trend in $\text{pCO}_{2\text{air}}$ was also observed (Figure 7h), which has been increasingly higher than in $\text{pCO}_{2\text{sea}}$. The increase in $\text{pCO}_{2\text{air}}$ may be caused by the high concentration of anthropogenic CO_2 present in the air, which is not being captured by the ocean with the same efficiency as before. Previous studies that modeled future scenarios already expected this response from the SO to increased CO_2 emissions (Sabine and Cols., 2004; Friedlingstein et al., 2006; Roy et al., 2011; Arora et al., 2013; Steinacher et al., 2013; Zickfeld et al., 2013). These models predicted that in scenarios with high greenhouse gas emissions, there would be a reduction in the efficiency of absorption by the ocean. The weakening of CO_2 absorption by the SO is due to the existence of a natural limit in gas exchange at the atmosphere-ocean interface, CO_2 dissociation, turbulent mixing and ocean circulation, which causes only a certain percentage of excess CO_2 atmospheric pressure to be absorbed. Therefore, although oceanic absorption is increasing, there are still high concentrations of CO_2 in the atmosphere (Le Quéré et al., 2013; IPCC, 2013; Heinze et al., 2015).

CO_2 absorption increased by $0.076 \text{ gC m}^{-2}\text{month}^{-1}$, from 2003 to 2022. Winds were intense, averaging 11.1 m/s (Figure 7g). The SST was higher than the air temperature ($\text{SST} > \text{Tair}$) throughout the studied period (Figure 7b), which indicates that the Marine Atmospheric Boundary Layer (CLAM) in this region is unstable and that an intense exchange of CO_2 occurs, as suggested by Pezzi et al. (2009).

The months 05/2005, 05/2007, 06/2009, 06/2011, 06/2015, 07/2019 and 07/2021 had absorption anomalies (FCO_2 varying from $0.075 \text{ gC m}^{-2}\text{month}^{-1}$ to $0.2 \text{ gC m}^{-2}\text{month}^{-1}$) (Figure 7a), that is, absorption was more intense in these periods than the expected average. These periods showed that the high negative values of FCO_2 were due to high values of SLP (ranging from 1008 hPa to 1013 hPa) and low values of SST (ranging from 8°C to 10°C) and Tar (ranging from 4.7°C to 6.7°C), intense winds (ranging from 11 m/s to 12.3 m/s), which caused the exchange of CO_2 at the ocean surface to be greater, with K varying from 18 to 33. However, on 02/2013 (FCO_2 $0.0134 \text{ gC m}^{-2}\text{month}^{-1}$) CO_2 absorption was lower than the expected average, due to low SLP values (1006 hPa) and wind speed, warmer SST and Tair, which caused gas transfer at the ocean-atmosphere interface to be lower, the K was 4.8.

Interannual variations are related to the phase variation of OA and ENSO, as observed by Lovenduski et al., 2008, Lenton et al., 2009, Brown et al., 2019, Costa et al., 2020 and Avelina et al., 2020. The months when intense reduction in CO_2 absorption occurred, such as 02/2013, had the influence of positive OA (+OA). +OA is defined by negative geopotential height and temperature anomalies. +OA increases the strength of westerly winds that lead to an increase in the upwelling of natural carbon from the depths of the ocean to the surface, causing a reduction in CO_2 absorption. However, the opposite occurred in the months 05/2005, 05/2007, 06/2009, 06/2011, 06/2015, 07/2019 and 07/2021, which had intense CO_2 absorption, a period of -OA (Gupta and England, 2006; Scholfield et al., 2018; Meredith et al., 2017; Keppler and Landschützer, 2019; Nevison et al., 2020). Furthermore, 06/2015, despite being a +OA month, was the most extreme El Niño period since 1998 (Monteiro et al., 2020). In this case, the role of El Niño was greater than that of OA. During El Niño, there is an increase in the mixing of Deep Circumpolar Waters with Dense Shelf Water advected from the Weddell Sea, leading to greater absorption of CO_2 . The opposite occurs in La Niña (Scholfield et al., 2018; Meredith et al., 2017; Brown et al., 2019; Keppler and Landschützer, 2019; Nevison et al., 2020; Costa et al., 2020; Avelina et al., 2020). The change in OA phase influences the flux variability, being able to increase

(negative phase) or reduce (positive phase) the absorption of CO_2 . ENSO becomes the main influence only in periods of strong intensity, as occurred in 06/2015. Therefore, most of the time the main modulator of FCO_2 is OA.

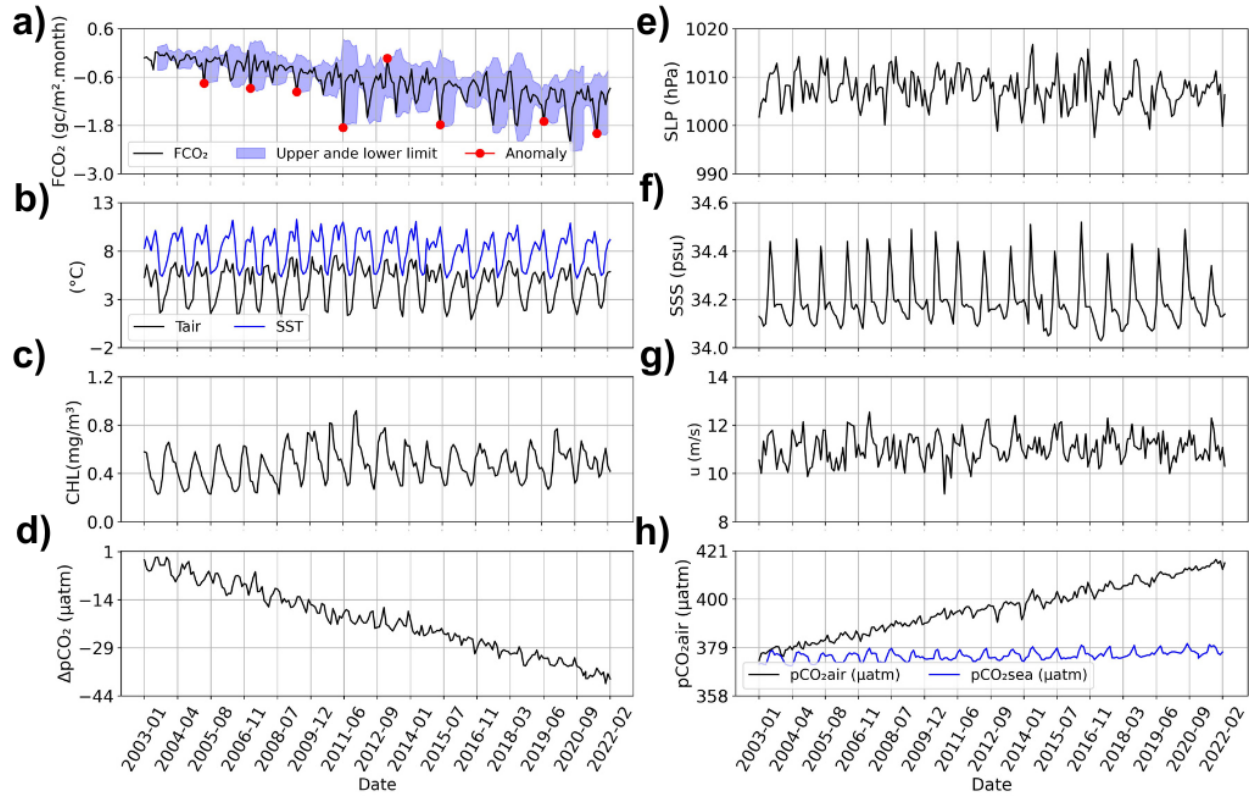


Figure 7 – Time series of atmospheric and oceanographic variables in the Drake Passage, from 2003 to 2022. CO_2 flux (FCO_2) (a), sea surface temperature (SST) and air temperature (Tair) (b), chlorophyll-a concentration (CHL) (c), difference of CO_2 partial pressure between the ocean and the atmosphere (ΔpCO_2) (d), atmospheric pressure at sea level (SLP) (e), salinity surface water (SSS) (f), wind speed (u) (g), seawater partial pressure of CO_2 ($\text{pCO}_{2\text{sea}}$), atmospheric partial pressure of CO_2 ($\text{pCO}_{2\text{air}}$) (h).

4 Final remarks and conclusions

This study showed the spatio-temporal variability on the sea-air FCO_2 caused by the ocean and atmosphere conditions, in the Atlantic sector of the Southern Ocean. The FCO_2 calculated through EC method using in situ data collected by ATMOS project (Pezzi et al. 2021; Voermans et al., 2021, Rodrigues, et al., 2023) offered a new source of atmospheric and oceanic data for CO_2 , heat and momentum in the Atlantic Sector of the Southern Ocean.

Monthly maps of FCO_2 were produced using an ANN for estimating $\text{pCO}_{2\text{sea}}$ with satellite and reanalysis data from 2003 to 2022. The absolute error between the FCO_2 produced from ANN and that produced with *in situ* data was $-1.3 \mu\text{mol}/\text{m}^2/\text{month}$ and the correlation was high ($r = 0.9$). This corresponds to a slight overestimation of 5.3% compared to the 31% obtained by Gloege et al., (2021) in the SO.

The FCO_2 varies from -0.05 to $0.05 \text{ gC m}^{-2}\text{month}^{-1}$ in the Atlantic sector of the SO, with the strongest CO_2 sink occurring in the summer and spring periods, and a lower sink in the austral winter and autumn. The seasonal variation of FCO_2 is modulated by changes in SST, in the Atlantic sector of the SO. In summer absorption is more intense than in other seasons, the peak occurs mainly in February. Summer absorption is 72% greater than in autumn and winter, and 51% greater than in the southern spring. The lowest absorption values occur mainly in August (winter). This is due to the expansion of sea ice cover that occurs in autumn and winter, with maximum expansion in August and September.

From 2003 to 2022, CO_2 absorption has intensified by $0.076 \text{ gC m}^{-2}\text{month}^{-1}$. In summer, absorption increased by $0.093 \text{ gC m}^{-2}\text{month}^{-1}$ compared to 2003 to 2022. In autumn, winter and spring the increase was $0.11 \text{ gC m}^{-2}\text{month}^{-1}$, $0.14 \text{ gC m}^{-2}\text{month}^{-1}$ and $0.1 \text{ gC m}^{-2}\text{month}^{-1}$, respectively, from 2003 to 2021.

During the study period, FCO_2 varied spatially, shaped by the characteristics of ocean fronts. The areas of the SF, because they have warm and saline waters, act as a source. Areas between the SF and the SAF, characterized by moderate SST and SSS, and intense winds, have strong absorption. Finally, there are areas with moderate absorption, located in the regions of the SB, in the SACCF and in the PF, which have colder and less saline waters.

The waters, which act as a source of CO_2 , are expanding southwards, and the waters, which act as sinks, have been intensifying the absorption of CO_2 . This is due to the increased strength and southward displacement of the westerly winds, associated with the positive trend of the AO, which forced the migration of the SF towards the Antarctic continent. Thus, warm and saline waters migrate and cause the release of CO_2 . In addition, the intensification of westerly winds on the circumpolar oceanic fronts intensifies the absorption of CO_2 in this region. The influence of ENSO only overlaps with the influence of the OA phase in periods of extreme ENSO, such as what occurred in 2015.

The results of this study show that FCO_2 in the SO are highly dependent on oceanographic and meteorological conditions. The spatial variation of FCO_2 is affected by the displacement of water masses. In addition, the intensification of westerly winds in the SAF, which increases gas exchange at the ocean-atmosphere interface, intensifies the absorption of CO_2 in this region. It also supports previous studies that modeled future scenarios on the reduction in the efficiency of CO_2 absorption by the ocean as a response by the Southern Ocean to the increase in greenhouse gas emissions. The ANN model for $\text{pCO}_{2\text{sea}}$ estimates is a very important tool to fill data gaps of $\text{pCO}_{2\text{sea}}$ in difficult-to-access areas, such as the SO, mainly in winter and southern autumn periods. It is also evident that the continuity of *in situ* sampling in this region with high quality data will allow us to improve the models produced and the understanding of the role of dynamic and thermodynamic processes that act as modulating mechanisms of CO_2 fluxes at the ocean-atmosphere interface of the Atlantic sector of the Southern Ocean.

Acknowledgments

The authors thank the Brazilian Navy, the Brazilian Ministry of Science, Technology and Innovations (MCTI), the Brazilian Antarctic Program (PROANTAR) for making the ATMOS 2.0 project and cruises possible and enjoyable. This research was funded by the Brazilian agencies CNPq, through the following projects: (i) Antarctic Modeling and Observation System

(CNPq/PROANTAR 443013/2018-7). (ii) The study of the Antarctic Climate, the Southern Ocean, and their relations with the Brazilian and South American environment (ATMOS 2.0) (CNPq/PROANTAR 440848/2023-7). L.P.P. is partly funded through a CNPq Scientific Productivity Fellowship (CNPq/303981/2023-7). The authors also acknowledge the support from the Graduate Program in Remote Sensing (PGSER) from the National Institute for Space Research (INPE).

Open Research

The Artificial Neural Network (ANN) software was designed to estimate pCO₂sea. The ANN used in the article can be found at <https://doi.org/10.5281/zenodo.10854860>, and can be developed openly in Python 3. Data from the meteorological tower installed on the bow of the Brazilian Navy Polar Ship (Po/V) Almirante Maximiano (H-41) were used to calculate the CO₂ flux (FCO₂) in the EddyPro®v7.0.9 software. These available data are in Carvalho, G. T., & Pezzi, L. P., 2024 (<https://doi.org/10.5281/zenodo.10871385>). LI-COR (LI-850) data installed in the laboratory aft of the Brazilian Navy Polar Ship (Po/V) Almirante Maximiano (H-41) were used to calculate pCO₂sea, available in Carvalho, G. T., & Pezzi, L. P., 2024 (<https://doi.org/10.5281/zenodo.10887055>).

References

- Arrigo, k. R., and g. L. Van dijen (2007), Interannual variation in air-sea CO₂ flux in the Ross Sea, Antarctica: A model analysis, *J. Geophys. Res.*, 112, C03020, doi:10.1029/2006JC003492
- Avelina R, da Cunha Lc, Farias Co, Hamacher C, Kerr R & Mata Mm. 2020. Contrasting dissolved organic carbon concentrations in the Bransfield Strait, northern Antarctic Peninsula: insights into ENOS and SAM effects. *J Mar Syst* 212: 1-51. <https://doi.org/10.1016/j.jmarsys.2020.103457>.
- Bakker, Dce, Pfeil, B., Landa, Cs, Metzl, N., O'brien, Km, Olsen, A., et al. (2016) A multi-decade record of high quality fCO₂ data in version 3 of the Surface Ocean CO₂ Atlas (SOCAT). *Earth System Science Data*, 8: 383-413. doi:10.5194/essd-8-383-2016
- Benallal, M.A.; Moussa, H.; Lencina-Avila, J.M.; Touratier, F.; Goyet, C.; JAI, M.C. El; POISSON, N.; POISSON, A.. Satellite-derived CO₂ flux in the surface seawater of the Austral Ocean south of Australia. *International Journal Of Remote Sensing*, [S.L.], v. 38, n. 6, p. 1600-1625, 6 fev. 2017. Informa UK Limited. <http://dx.doi.org/10.1080/01431161.2017.1286054>.
- Brown, Michael S.; Munro, David R.; Feehan, Colette J.; Sweeney, Colm; Ducklow, Hugh W.; Schofield, Oscar M.. Enhanced oceanic CO₂ uptake along the rapidly changing West Antarctic Peninsula. *Nature Climate Change*, [S.L.], v. 9, n. 9, p. 678-683, 26 ago. 2019. *Springer Science and Business Media LLC*. <http://dx.doi.org/10.1038/s41558-019-0552-3>.
- Cai, W.J., Cowan, T. (2007). Trends in Southern Hemisphere circulation in IPCC AR4 models over 1950-99: Ozone-depletion vs. greenhouse forcing, *Journal of Climate*, 20(4), 681–693.
- Carvalho, G. T. and Mejia, C. (2024). Artificial Neural Network (ANN) to estimate pCO₂sea. (Version 1.1.0) [Software]. (RNApCO₂sea-Carvalho). Zenodo. <https://doi.org/10.5281/zenodo.10854860>

- Carvalho, G. T., & Pezzi, L. P. (2024). Data from the micrometeorological tower of the Antarctic Modeling Observation System (ATMOS) project of the 40th Brazilian Antarctic Operation (OPERANTAR XL) to calculate the CO₂ flux (FCO₂) [Data set]. Zenodo. <https://doi.org/10.5281/zenodo.10871385>
- Carvalho, G. T., & Pezzi, L. P. (2024). LI-COR (LI-850) sensor data obtained by the Antarctic Modeling Observation System (ATMOS) project during the 40th Brazilian Antarctic Operation (OPERANTAR XL) and were used to calculate the partial pressure of CO₂ (pCO₂) [Data set]. Zenodo. <https://doi.org/10.5281/zenodo.10887055>
- Chahine, M., Barnet, C., Olsen, E.T., Chen, L., Maddy, E., 2005. On the determination of atmospheric minor gases by the method of vanishing partial derivatives with application to CO₂: DETERMINATION OF MINOR GASES BY VPD. *Geophys. Res. Lett.* 32 <https://doi.org/10.1029/2005gl024165>.
- Chatterjee A., Gierach MM, Sutton AJ, Feely RA, Crisp D., Eldering A., Gunson MR, O'Dell CW, Stephens BB, Schimel DS. Influence of El Nino on atmospheric CO₂ over tropical Pacific Ocean: Findings from NASA's OCO-2 mission, *Science* 13 out 2017, Vol. 358, Issue 6360, eaam5776 DOI: 10.1126/science.aam5776.
- Chollet, f. (2018). *Deep Learning with Python (First)*. Manning Publications Co.
- Clowes, A.J. Influence of the Pacific on the circulation in the South-West Atlantic Ocean. *Nature*, v. 131, p. 189-191, 1933.
- Cook, A. J., FOX, A. J., VAUGHAN, D. G. & FERRIGNO, J. G. Retreating glacier fronts on the Antarctic Peninsula over the past half-century. *Science* 308, 541–544 (2005).
- Costa, R. R. et al. Dynamics of an intense diatom bloom in the Northern Antarctic Peninsula, February 2016. *Limnol. Oceanogr.* 66, 1–20 (2020).
- Dejong, Hb & Dunbar, Rb. Air-sea CO₂ exchange in the Ross Sea, Antarctica. *J. Geophys. Res. Oceano* 122 , 8167-8181 (2017).
- Ducklow, H. W. et al. West Antarctic Peninsula: an ice-dependent coastal marine ecosystem in transition. *Oceanography* 26, 190–203 (2013).
- Farias, E. G. G.; Nobre, P.; Lorenzetti, J. A.; Almeida, R. A. F.; Junior, L. C. I. Variability of air-sea CO₂ fluxes and dissolved inorganic carbon distribution in the Atlantic basin: a coupled model analysis. *International Journal of Geosciences*, v. 2013, p. 249–258, 2013.
- Fogt, Ryan L.; Marshall, Gareth J.. The Southern Annular Mode: variability, trends, and climate impacts across the southern hemisphere. *Wires Climate Change*, [S.L.], v. 11, n. 4, p. 1-24, 19 maio 2020. Wiley. <http://dx.doi.org/10.1002/wcc.652>.
- Géron, Aurélien. *Hands-on machine learning with Scikit-Learn and TensorFlow: concepts, tools, and techniques to build intelligent systems*. [S.l.]: "O'Reilly Media, Inc.", 2017.
- Goldemberg, José et al. *Antarctica and global changes: a challenge for humanity*. Publishing company Blucher, 2011.
- Hackerott, J. A. et al. The role of roughness and stability on the momentum flux in the marine atmospheric surface layer: A study on the southwestern Atlantic Ocean. *J. Geophys. Res. Atmos.* 123, 3914–3932. <https://doi.org/10.1002/2017JD027994> (2018).
- Hadjer, M. & Benallal, Mohamed & Goyet, Catherine & Lefèvre, Nathalie. (2016). Satellite-derived CO₂ fugacity in surface seawater of the tropical Atlantic Ocean using a feedforward neural network. *International Journal of Remote Sensing*. 37. 580–598. [10.1080/01431161.2015.1131872](https://doi.org/10.1080/01431161.2015.1131872)

- Heinze, C., Meyer, S., Goris, N., Anderson, L., Steinfeldt, R., Chang, N., Le Quéré, C., And Bakker, D. C. E.: The ocean carbon sink – impacts, vulnerabilities and challenges, *Earth Syst. Dynam.*, 6, 327–358, <https://doi.org/10.5194/esd-6-327-2015>, 2015.
- IPCC – Intergovernmental Panel on Climate Change, Working Group I Contribution to the Fifth Assessment Report, *Climate Change 2013 – the Physical Science Basis*.
- Ito, R. G.; Garcia, C. A. E.; Tavano, V. M.. Net sea-air CO₂ fluxes and modelled pCO₂ in the southwestern subtropical Atlantic continental shelf during spring 2010 and summer 2011. *Continental Shelf Research*, [S.L.], v. 119, p. 68-84, maio 2016. Elsevier BV. <http://dx.doi.org/10.1016/j.csr.2016.03.013>.
- Keppler & Landschützer P. 2019. Regional wind variability modulates the Southern Ocean carbon sink. *Sci Rep* 9(1): 1-10. <https://doi.org/10.1038/s41598-019-43826-y>.
- Klinck, J. M., and W. D. Nowlin Jr. (2001), Antarctic Circumpolar Current, in *Encyclopedia of Ocean Science*, 1st ed., pp. 151–159, Academic, San Diego, Calif.
- Landschützer, P.; Gruber, N.; Bakker, D. C. E.; Schuster, U.; Nakaoka, S.; Payne, M. R.; Sasse, T. P.; Zeng, J.. A neural network-based estimate of the seasonal to inter-annual variability of the Atlantic Ocean carbon sink. *Biogeosciences*, [S.L.], v. 10, n. 11, p. 7793-7815, 29 nov. 2013. Copernicus GmbH. <http://dx.doi.org/10.5194/bg-10-7793-2013>.
- Landschutzer, P., et al. (2015), The reinvigoration of the Southern Ocean carbon sink, *Science*, 349, 6253.
- Le Quéré, C., et al. Saturation of the Southern Ocean CO₂ sink due to recent climate change, *Science*, 316, 1735–1738, 2007.
- Le Quéré, C., Andres, R. J., Boden, T., Conway, T., Houghton, R. A., House, J. I., Marland, G., Peters, G. P., van der Werf, G. R., Ahlström, A., Andrew, R. M., Bopp, L., Canadell, J. G., et al.: The global carbon budget 1959–2011, *Earth Syst. Sci. Data*, 5, 165–185, <https://doi.org/10.5194/essd-5-165-2013>, 2013.
- Lovenduski, N. S., N. Gruber, and S. C. Doney (2008), Toward a mechanistic understanding of the decadal trends in the Southern Ocean carbon sink, *Global Biogeochem. Cycles*, 22, GB3016, doi:10.1029/2007GB003139.
- Mcgillis, W.R., Edson, J.B., Fairall, C.W., 2001. Direct covariance air-sea CO₂ fluxes. *J. Geophys. Res.* 106, 16,729–16,745.
- Meijers, Ajs (2014). The Southern Ocean in the Phase-5 Coupled Model Intercomparison Project. *Philosophical Transactions of the Royal Society of London, Series A: Mathematical, Physical and Engineering Sciences*, 372 (2019), 20130296. <https://doi.org/10.1098/rsta.2013.0296>
- Meredith et al. Changing distributions of sea ice melt and meteoric water west of the Antarctic Peninsula. *Deep Sea Res. Pt II* 139, 40–57 (2017).
- Miller, S. D. et al. Platform motion effects on measurements of turbulence and air-sea exchange over the open ocean. *Journal of Atmospheric and Oceanic Technology*, v. 25, n. 9, p. 1683–1694, 2008.
- Monteiro, T., Kerr, R. & Machado, E.D. Seasonal variability of net sea-air CO₂ fluxes in a coastal region of the northern Antarctic Peninsula. *Sci Rep* 10, 14875 (2020). <https://doi.org/10.1038/s41598-020-71814-0>
- Moussa, H., M. A. Benallal, C. Goyet, And N. Lefèvre. 2016. Satellite-Derived CO₂ Fugacity in Surface Seawater of the Tropical Atlantic Ocean Using a Feedforward Neural Network. *International Journal of Remote Sensing* 37 (3): 580–598. doi:10.1080/01431161.2015.1131872.

- Nakaoka, S., Telszewski, M., Nojiri, Y., Yasunaka, S., Miyazaki, C., Mukai, H., and Usui, N.: Estimating temporal and spatial variation of ocean surface pCO₂ in the North Pacific using a self-organizing map neural network technique, *Biogeosciences*, 10, 6093–6106, <https://doi.org/10.5194/bg-10-6093-2013>, 2013.
- Nevison, C. D.; Munro, D. R.; Lovenduski, N. S.; Keeling, R. F.; Manizza, M.; Morgan, E. J.; Rödenbeck, C.. Southern Annular Mode Influence on Wintertime Ventilation of the Southern Ocean Detected in Atmospheric O₂ and CO₂ Measurements. *Geophysical Research Letters*, [S.L.], v. 47, n. 4, p. 1-9, 17 fev. 2020. American Geophysical Union (AGU). <http://dx.doi.org/10.1029/2019gl085667>.
- Nomura, D., Yoshikawa-Inoue, H., Toyota, T., 2006. The effect of sea-ice growth on air–sea CO₂ flux in a tank experiment. *Tellus* 58 B, 418–426.
- Parkinson, C. L. and Cavalieri, D. J.: Antarctic sea ice variability and trends, 1979–2010, *The Cryosphere*, 6, 871–880, <https://doi.org/10.5194/tc-6-871-2012>, 2012.
- Parkinson, C. L. 40–y record reveals gradual Antarctic sea ice increases followed by decreases at rates far exceeding the rates seen in the Arctic. *Proceedings of the National Academy of Sciences* 116(29): 14414–14423. <https://doi.org/10.1073/pnas.1906556111>. 2019.
- Pezzi, L. P.; Souza, R. B.; Acevedo, O.; Wainer, I.; Mata, M. M.; Garcia, C. A. E.; Camargo, R. Multiyear measurements of the oceanic and atmospheric boundary layers at the Brazil-Malvinas confluence region. *Journal of Geophysical Research Atmospheres*, v. 114, n. 19, p. 1–19, 2009.
- Pezzi, L.P., de Souza, R.B., Santini, M.F. et al. Oceanic eddy-induced modifications to air–sea heat and CO₂ fluxes in the Brazil-Malvinas Confluence. *Sci Rep* 11, 10648 (2021). <https://doi.org/10.1038/s41598-021-89985-9>
- Rodrigues, C. C. F., Santini, M. F., Lima, L. S., Sutil, U. A., Carvalho, J. T., Cabrera, M. J., Rosa, E. B., Burns, J. W., & Pezzi, L. P.. (2023). Ocean-atmosphere turbulent CO₂ fluxes at Drake Passage and Bransfield Strait. *Anais Da Academia Brasileira De Ciências*, 95, e20220652. <https://doi.org/10.1590/0001-3765202320220652>
- Rodrigues C.C.F., Santini, M.F., Brunsell, N.A., Pezzi, L.P. (2024). CO₂ fluxes under different oceanic and atmospheric conditions in the Southwest Atlantic Ocean. *Journal of Marine Systems* 243, 2024, 03949. <https://doi.org/10.1016/j.jmarsys.2023.103949>.
- Sabine, C. L.; Hankin, S.; Koyuk, H.; Bakker, D. C. E.; Pfeil, B.; Olsen, A.; Metzl, N.; Kozyr, A.; Fassbender, A.; Manke, A.. Surface Ocean CO₂ Atlas (SOCAT) gridded data products, *Earth System Science Data*, [S.L.], v. 5, n. 1, p. 145–153, 4 abr. 2013. Copernicus GmbH. <http://dx.doi.org/10.5194/essd-5-145-2013>.
- Santini, M. F., Souza, R. B., Pezzi, L. P. & Swart, S. Observations of air-sea heat fluxes in the Southwestern Atlantic under highfrequency ocean and atmospheric perturbations. *Q. J. R. Meteorol. Soc.* <https://doi.org/10.1002/qj.3905> (2020).
- Santini, M. F., Souza, R. B., Wayner, I. K. & Muelbert, M. Temporal analysis of water masses and sea ice formation rate west of the Antarctic Peninsula in 2008 estimated from southern elephant seals' SRDL–CTD data. *Deep Sea Res. Part II Top. Stud. Oceanogr.* (2018)
- Silva, L. A.; Andrade, J. B. D.; Lopes, W. A.; Carvalho, L. S.; Pereira, P. A. P.. Solubility and reactivity of gases. *New Chemistry*, [S.L.], p. 824–832, 24 mar. 2017. *Sociedade Brasileira de Química (SBQ)*. <http://dx.doi.org/10.21577/0100-4042.20170034>.
- Sutton, A. J.; Williams, N. L.; Tilbrook, B.. Constraining Southern Ocean CO₂ Flux Uncertainty Using Uncrewed Surface Vehicle Observations. *Geophysical Research Letters*, [S.L.], v. 48,

- n. 3, p. 1-9, 9 fev. 2021. American Geophysical Union (AGU).
<http://dx.doi.org/10.1029/2020gl091748>.
- Takahashi, T.; Sutherland, S. C.; Wanninkhof, R.; Sweeney, C.; Feely, R. A.; Chipman, D.W.; Hales, B.; Friederich, G.; Chavez, F.; Sabine, C.. Climatological mean and decadal change in surface ocean pCO₂, and net sea–air CO₂ flux over the global oceans. *Deep Sea Research Part II: Topical Studies in Oceanography*, [S.L.], v. 56, n. 8-10, p. 554-577, abr. 2009. Elsevier BV. <http://dx.doi.org/10.1016/j.dsr2.2008.12.009>.
- Talley, L. D., Reid, J. L. & Robbins, P. E. 2003. Data-based meridional overturning streamfunctions for the global ocean. *J. Clim.* 16, 3213–3226.
- Taylor, K. E. Summarizing multiple aspects of model performance in a single diagram. *Journal of Geophysical Research*, v.106, n.7, p.7183-7192, 2001.
- Thompson, D. W. J.; Wallace, J. M.. Annular Modes in the Extratropical Circulation. Part I: month-to-month variability*. *Journal Of Climate*, [S.L.], v. 13, n. 5, p. 1000-1016, mar. 2000. American Meteorological Society. [http://dx.doi.org/10.1175/1520-0442\(2000\)0132.0.co;2](http://dx.doi.org/10.1175/1520-0442(2000)0132.0.co;2).
- Turner, J. et al. Antarctic climate change and the environment: an update. *Polar Rec.* 50, 237–259 (2014).
- Viana, D. De L.; Oliveira, J. E. L.; Hazin, F. H. V.; Souza, M. A. C.; Marine sciences: from the world's oceans to northeast Brazil. Olinda (PE): Via Design Publicações, 2021. 512 p.
- Voermans, J. J., Babanin, A., Kirezci, C., Carvalho, J. T., Santini, M. F., Pavani, B. F. And Pezzi, L. P. Wave Anomaly Detection in Wave Measurements. *J. Atmos. Ocean. Technol.* 38, 525–536 (2021).. DOI: <https://doi.org/10.1175/JTECH-D-20-0090.1>
- Wadhams, P. Ice in the ocean. Amsterdam: Gordon and Breach Science Publishers. 351 p. 2000.
- Wallace, J.M.; Hobbs, P.V. *Atmospheric Science: An Introductory Survey* 2 ed., London Academic Press, 2006, 483 p.
- Wanninkhof, R. Relationship between wind speed and gas exchange over the ocean revisited. *Limnology and Oceanography: Methods*, v. 12, p. 351– 362, 2014.
- Weiss, A.; Kuss, J.; Peters, G.; Schneider, B. Evaluating transfer velocity wind speed relationship using a long-term series of direct eddy correlation CO₂ flux measurements. *Journal of Marine Systems*, v. 66, n. 1/4, p. 130-139, 2007.
- Weiss, R. F. Carbon dioxide in water and seawater: the solubility of a non-ideal gas. *Marine Chemistry*, Amsterdam, v. 2, p. 203-215, 1974.
- Zeng, J.; Nojiri, Y.; Landschützer, P.; Telszewski, M.; Nakaoka, S.. A Global Surface Ocean fCO₂ Climatology Based on a Feed-Forward Neural Network. *Journal Of Atmospheric And Oceanic Technology*, [S.L.], v. 31, n. 8, p. 1838-1849, 1 ago. 2014. *American Meteorological Society*. <http://dx.doi.org/10.1175/jtech-d-13-00137.1>.